ACS APPLIED MATERIALS & INTERFACES

Research Article

www.acsami.org

Reduced Graphene Oxide Modified Li_2FeSiO_4/C Composite with Enhanced Electrochemical Performance as Cathode Material for Lithium Ion Batteries

Lu-Lu Zhang,[†] Song Duan,[†] Xue-Lin Yang,*[,†] Gang Peng,[†] Gan Liang,[‡] Yun-Hui Huang,[§] Yan Jiang,[§] Shi-Bing Ni,[†] and Ming Li[†]

[†]College of Mechanical and Material Engineering, Collaborative Innovation Center for Energy Equipment of Three Gorges Region, Three Gorges University, 8 Daxue Road, Yichang, Hubei 443002, China

[‡]Department of Physics, Sam Houston State University, Huntsville, Texas 77341, United States

[§]School of Materials Science and Engineering, State Key Laboratory of Material Processing and Die & Mould Technology, Huazhong University of Science and Technology, 1037 Luoyu Road, Wuhan, Hubei 430074, China

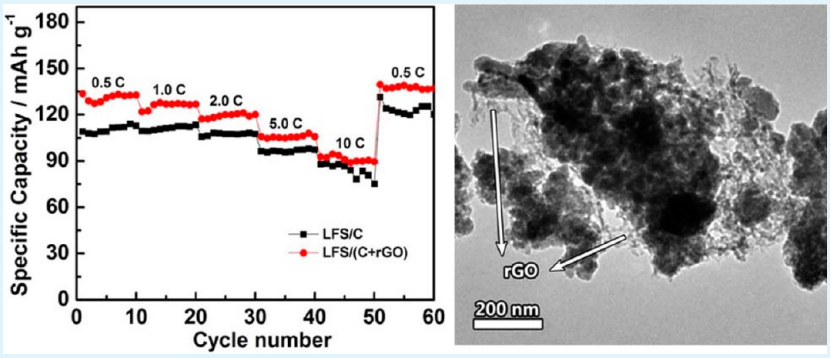

ABSTRACT: Reduced graphene oxide modified Li_2FeSiO_4/C (LFS/(C+rGO)) composite is successfully synthesized by a citric-acid-based sol−gel method and evaluated as cathode material for lithium ion batteries. The LFS/(C+rGO) shows an improved electronic conductivity due to the conductive network formed by reduced graphene oxide nanosheets and amorphous carbon in particles. Electrochemical impedance spectroscopy results indicate an increased diffusion coefficient of lithium ions (2.4×10^{-11} cm^2 s^{-1}) for LFS/(C+rGO) electrode. Compared with LFS with only amorphous carbon, the LFS/(C+rGO) electrode exhibits higher capacity and better cycling stability. It delivers a reversible capacity of 178 mAh g^{-1} with a capacity retention ratio of 94.5% after 40 cycles at 0.1 C, and an average capacity of 119 mAh g^{-1} at 2 C. The improved performance can be contributed to the reduced crystal size, good particle dispersion, and the improved conductive network between LFS particles.

KEYWORDS: *lithium ion battery, cathode material, Li_2FeSiO_4, reduced graphene oxide, electrochemical performance*

1. INTRODUCTION

Nowadays the increasing consumption of fossil fuel drives people to look for new alternative energy resources. For instance, lithium-ion batteries (LIBs) have attracted increasing attention due to their high operating voltage, high energy density, long cycle life, low self-discharge, nonmemory effect, and so forth. As an important component of LIBs, cathode material always arouses more attention due to the key role in improving electrochemical performance and reducing the cost of the whole cell.[1] Since Nytén et al. first explored Li_2FeSiO_4 (LFS) as a new cathode material for LIBs, LFS has attracted wide interest due to its low cost, high safety, environmentally benign character, and high theoretical capacity (166 mAh g^{-1} for one Li^+ ion exchange, and 332 mAh g^{-1} for two Li^+ ions exchange).[2−5] However, as a polyanion cathode material, LFS suffers from poor capability due to its poor intrinsic electronic conductivity and slow lithium ion diffusion rate, which limits its large scale application in LIBs. Therefore, much effort has been made to improve the electrochemical performance of LFS, such as particle downsizing, carbon incorporation, and metal ion doping. Particularly, carbon incorporation appears to be one of the most effective methods. Various carbon sources, such as glucose,[6] sucrose,[7−9] citric acid,[10,11] and carbon nanotubes,[3,12,13] have been successfully used to improve the electrochemical performance of LFS.

Recently, graphene has been implemented as a new and promising electron conducting additive for cathode materials of LIBs, because graphene can form a 3D electron conducting network in cathode materials to increase electron conductivity.[14] The reduced graphene oxide (denoted as rGO) sheets are

Received: June 23, 2013
Accepted: November 6, 2013
Published: November 6, 2013

Figure 1. Schematic illustration of the synthesis process for LFS/(C+rGO) composite.

usually considered as one kind of chemically derived graphene.[15] In current research, graphene and rGO are found to significantly improve the rate capability and cyclability of some cathode materials such as $LiFePO_4$, $Li_3V_2(PO_4)_3$, $LiMn_2O_4$, and so forth.[16−22] However, up to now, there is no report about the rGO-modification for Li_2FeSiO_4 (LFS). In this work, rGO-modified LFS/C composite was prepared via a citric acid based sol−gel method, and characterized by X-ray diffraction (XRD), scanning electron microscopy (SEM), transmission electron microscopy (TEM), and Raman spectrometry. The effect of rGO on the electrochemical performance of LFS was also investigated.

2. EXPERIMENTAL SECTION

Reduced graphene oxide modified LFS/C composite was synthesized via sol−gel method. Citric acid was chosen as a chelating agent. First, $LiNO_3$, $Fe(NO_3)_3{\cdot}9H_2O$ and citric acid in stoichiometric molar ratio of 2:1:3 were successively dissolved in deionized water under stirring. Second, the aqueous solution of the mixture was transferred into an ethanol solution containing stoichiometric amount of tetraethyl orthosilicate (TEOS). Subsequently, graphene oxide (GO) prepared from natural graphite by a typical Hummers method[23] was added in the mixture under stirring, and the above mixture was refluxed at 70 °C for 12 h. After solvent evaporation and vacuum drying (120 °C, 12 h), a dry gel precursor was obtained. The obtained gel was then finely ground with sucrose in acetone for 6 h. After drying, the above mixture was calcined at 350 °C for 5 h, and then sintered at 650 °C for 10 h under flowing nitrogen gas to obtain the rGO modified LFS/C composite (denoted as LFS/(C+rGO)). The overall synthesis process for the LFS/(C+rGO) composite is schematically illustrated in Figure 1. For comparison, Li_2FeSiO_4/C composite was synthesized via the same process without GO (denoted as LFS/C). Noting that, in order to avoid the influence of total carbon amount on the electrochemical performance of LFS, the amount of sucrose for LFS/(C+rGO) is reduced accordingly so as to obtain the approximately equal residual carbon content in the two samples.

LFS/C and LFS/(C+rGO) composites were characterized by X-ray powder diffraction with Cu Kα radiation (λ = 1.5406 Å) (XRD, Rigaku Ultima IV). Diffraction patterns were scanned over the range of 2θ between 10° and 90° in a step of 0.02°. The morphology was observed with a field-scanning electron microscope (FSEM, JSM-7500F, JEOL) coupled with an energy dispersive X-ray (EDX) detector and a transmission electron microscope (TEM, JEM-2100, JEOL). Carbon coating on LFS/C and LFS/(C+rGO) powders was characterized by Raman spectrometry (VERTEX 70, Bruker). Residual carbon content in both samples was determined by a carbon sulfur analyzer (CS600, LECO, US). Electrical conductivity was measured with a standard four-probe method by RTS resistivity measurement system (RTS-8, China) on disk-shaped pellets with diameter of 8 mm and thickness of about 1.0 mm.

The working electrodes were prepared by mixing 75 wt % active materials (i.e., LFS/C and LFS/(C+rGO), respectively) with 15 wt % acetylene black and 10 wt % PVDF in *N*-methyl pyrrolidinone (0.02 g mL^{-1}). The above slurry was coated on an aluminum foil (20 μm in thickness) using an automatic film-coating equipment. The resulting film was dried under an infrared light to remove volatile solvent, punched into discs (φ14 mm), and then pressed under a pressure of 6 MPa. After drying at 120 °C for 12 h in vacuum, the discs were transferred into an argon-filled glovebox (Super 1220/750, Mikrouna). The loading of the active materials on the electrode was 1.8 mg cm^{-2}. 2025 coin cells were assembled using Celgard 2400 as the separator and lithium foil as counter and reference electrodes. A solution of 1 mol L^{-1} $LiPF_6$ in a 1:1 volumetric mixture of EC and DMC (LB-301, China) was employed as the electrolyte. The cells were tested between 1.5 and 4.8 V on a battery test system (LAND CT2001A, China). Electrochemical impedance spectroscopy (EIS) measurement was performed on an electrochemical working station (CHI614C, China) over a frequency range between 0.01 Hz and 100 kHz.

3. RESULTS AND DISCUSSION

Figure 2 shows the XRD patterns of LFS/C and LFS/(C+rGO) samples. In spite of two weak diffraction peaks for the

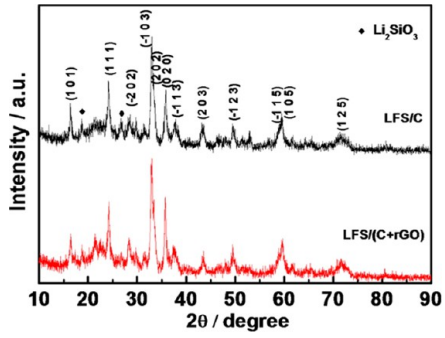

Figure 2. XRD patterns of LFS/C and LFS/(C+rGO) powders.

Li_2SiO_3 impurity phase, the main diffraction peaks for the two samples are well indexed as monoclinic structure of LFS with space group $P2_1/n$, which agrees well with previous reports.[5,24] The average crystal sizes of LFS/C and LFS/(C+rGO) samples are about 200 and 160 nm, respectively, which are calculated from the (111), (−103), and (020) planes of monoclinic Li_2FeSiO_4 based on Scherrer's equation. Obviously, rGO incorporation reduces the crystal size, which is helpful to shorten the transport path of Li^+ ions and improve the utilization of active materials. In addition, no peaks for crystalline carbon and GO are observed, suggesting that the carbon in the composite is in amorphous form and the GO has been reduced.[25] It is difficult to completely convert GO to graphene at 650 °C under N_2, but the GO can be easily converted to rGO.[15,26] The diffraction peaks at 2θ of around 24° and 43° correspond to the (002) and (100) peaks of the

disorderedly stacked rGO sheets, respectively,[27] which are overlapped with (111) and (203) peaks of LFS. The amount of residual carbon in both LFS/C and LFS/(C+rGO) samples is approximately 9 wt % as determined by a carbon−sulfur analyzer. The weight ratio of amorphous carbon to rGO in LFS/(C+rGO) composite is calculated to be 3:1. Amorphous carbon can act not only as conductive agent to improve the electronic conductivity of LFS, but also as reductive agent to reduce Fe^{3+} to Fe^{2+}; and a hybrid conductive network is formed by rGO nanosheets and amorphous carbon in LFS/(C+rGO) particles to further improve the electronic conductivity of LFS.

Figure 3 shows the SEM images of LFS/C and LFS/(C +rGO) samples. Compared to the LFS/C particles, the LFS/(C

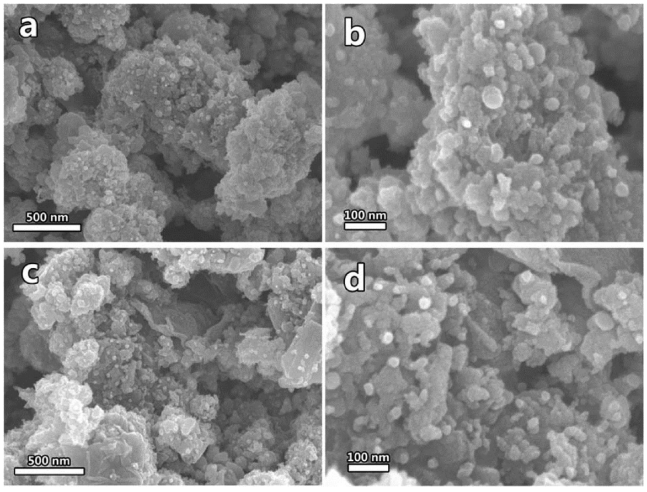

Figure 3. SEM images of the as-prepared samples: (a,b) LFS/C and (c,d) LFS/(C+rGO).

+rGO) particles present less agglomeration, which can be ascribed to the inhibition of agglomeration of fine particles not only by the pyrolytic carbon but also by the rGO. The morphology and structure of the two samples are further confirmed by TEM and HRTEM (Figure 4). It is clearly seen from Figure 4 that both samples are composed of small particles with size in the range of 50−100 nm. LFS/C particles are coated with or embedded in amorphous carbon decomposed from sucrose, and the thickness of the carbon layer is about 5−7 nm (Figure 4a and b). For LFS/(C+rGO) composite, the amorphous carbon is left on the surface not only of LFS particles (with a decreased thickness of 3−5 nm) but also of rGO sheets. The thin carbon layer in LFS/(C+rGO) particles caused by the reduced sucrose is more favorable for Li^+ ions transport. For LFS/(C+rGO) composite, LFS particles and rGO sheets are readily linked together with the residual amorphous carbon (Figure 4c and d), indicative of an improved conductive network among LFS particles. The electronic conductivity of LFS/(C+rGO) is measured to be 1.5×10^{-3} S cm^{-1}, whereas that of LFS/C is only 7.1×10^{-4} S cm^{-1}. The increased electronic conductivity for LFS/(C+rGO) indicates that the insulated GO is successfully reduced during heating process in N_2, which agrees well with the result from XRD analysis. Obviously, the hybrid conductive network formed by rGO nanosheets and amorphous carbon in LFS/(C+rGO) particles is more favorable for electron migration. Additionally, the clear crystal planes (with *d*-spacings of 0.34 and 0.24 nm corresponding to the (102) planes and the (−1−13) planes for Li_2FeSiO_4, respectively) in Figure 4b and d clearly confirm the

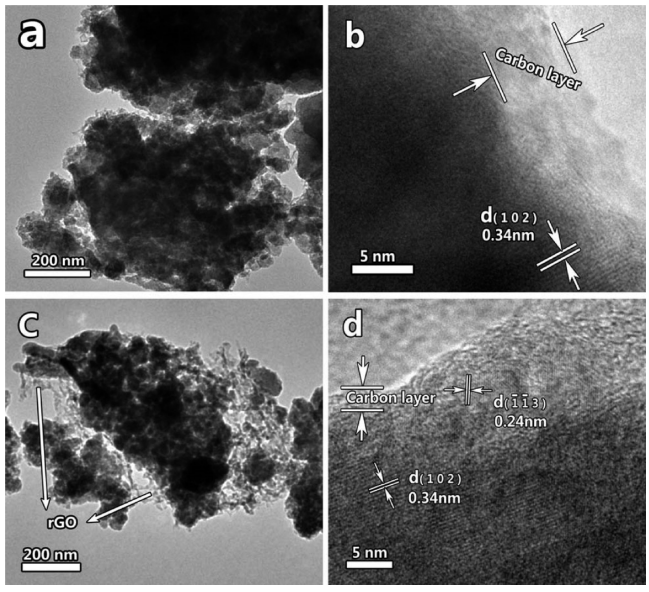

Figure 4. TEM images of the as-prepared samples: (a,b) LFS/C and (c,d) LFS/(C+rGO).

crystalline nature of monoclinic LFS in the LFS/C and LFS/(C +rGO) composites. In order to investigate the distribution of the component elements in the particles, the elemental mapping of Si, Fe, and C species in LFS/(C+rGO) sample was examined by EDX. As displayed in Figure 5, all the elements (Si, Fe, and C) show homogeneous distribution, which demonstrates that these elements are uniformly distributed in the LFS/(C+rGO) sample.

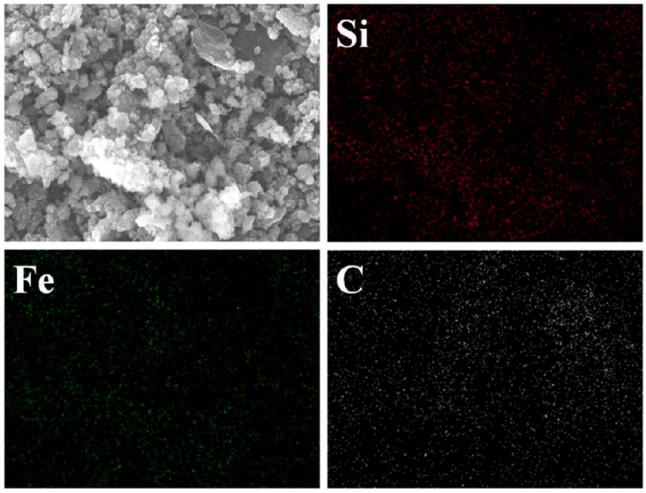

Figure 5. EDX mapping of LFS/(C+rGO) powders.

To investigate the effect of rGO on the electrochemical performance of LFS, galvanostatic charge−discharge tests on the LFS/C and LFS/(C+rGO) electrodes materials were performed in the voltage range of 1.5−4.8 V (vs Li^+/Li) under various C rates (1 C = 166 mAh g^{-1}) (Figures 6 and 7). Figure 6a shows the initial three charge−discharge profiles at 0.1 C for LFS/C and LFS/(C+rGO) electrodes. As shown in Figure 6a, two potential plateaus (~3.2 and ~4.5 V) can be found in the first charge curves for both samples, which agree well with the previous reports.[20,24,28−30] The first potential plateau (~3.2 V) corresponds to the Fe^{2+}/Fe^{3+} redox couple.[31]

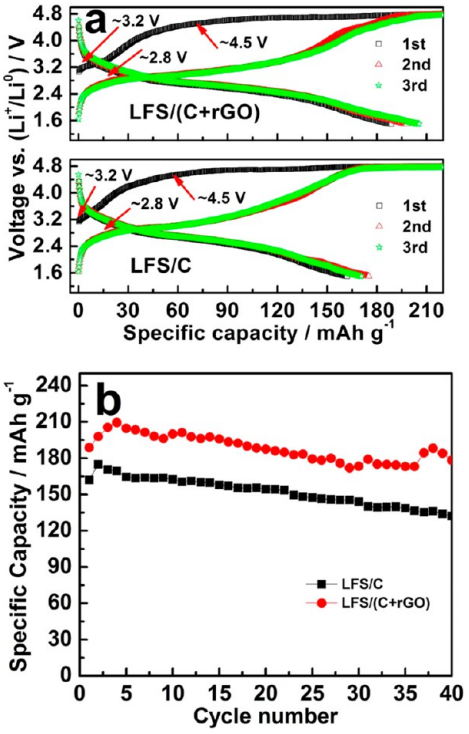

Figure 6. (a) First three charge/discharge profiles at 0.1 C and (b) cycle performance of LFS/C and LFS/(C+rGO) cycled at 0.1 C.

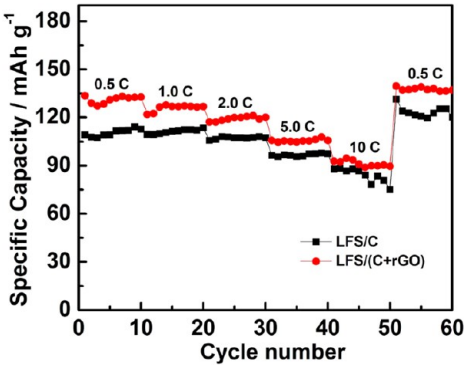

Figure 7. Rate capability of LFS/C and LFS/(C+rGO) electrodes.

However, due to polarization, the first potential plateau (~3.2 V) is less obvious.[20,24] Subsequently, the potential plateau at ~3.2 V shifts to ~2.8 V in the second charge process, indicative of a structural rearrangement.[31] The second voltage plateau (~4.5 V), disappeared in the following charge processes, should correspond to the Fe^{3+}/Fe^{4+} redox couple, which was proved by Lv et al.[28] On the further charge processes, the potential plateaus are stabilized at ~2.8 V, suggesting little or no subsequent change in structure. Compared to LFS/C (162.1 mAh g^{-1}), the LFS/(C+rGO) electrode delivers a higher initial discharge capacity of 188.7 mAh g^{-1} at 0.1 C, which corresponds to more than one Li^+ ions exchange. Figure 6b shows the cycling performance of LFS/C and LFS/(C+rGO) cycled at 0.1 C. In both cases, there is an increase in capacity within the initial several cycles and then a decrease in capacity. This is due to the gradual penetration of electrolyte into the electrode followed by the increased polarization effect. The LFS/(C+rGO) electrode delivers a reversible capacity of 178 mAh g^{-1} with a capacity retention ratio of 94.5% after 40 cycles, which is higher than that of LFS/C (132 mAh g^{-1}, 81.6%). Obviously, the LFS/(C+rGO) electrode exhibits enhanced capacity and cyclability.

Figure 7 shows the rate capability for LFS/C and LFS/(C+rGO) electrodes. The cells were cycled at different C rates from 0.5 to 10 C and then back to 0.5 C, each for 10 cycles. It can be clearly seen that the discharge capacity of both samples gradually decreases with increasing C-rate because of the increased polarization and the decreased utilization of active materials at high current density. The LFS/(C+rGO) electrode shows remarkably improved capability at any C-rate. It delivers an average capacity of 119 mAh g^{-1} at 2 C, which is higher than the LFS/C electrode (107 mAh g^{-1}). Noting that, the LFS/(C+rGO) electrode even remains at a slightly higher discharge capacity of 140 mAh g^{-1} than the initial discharge capacity (134 mAh g^{-1}) at 0.5 C after 50 cycles at different C-rate (from 0.5 to 10 C). It is obvious that rGO incorporation can effectively improve the electrochemical performance of LFS.

In order to understand the effect of rGO incorporation on the electrochemical performance of LFS, the EIS curves of LFS/C and LFS/(C+rGO) electrodes are shown in Figure 8.

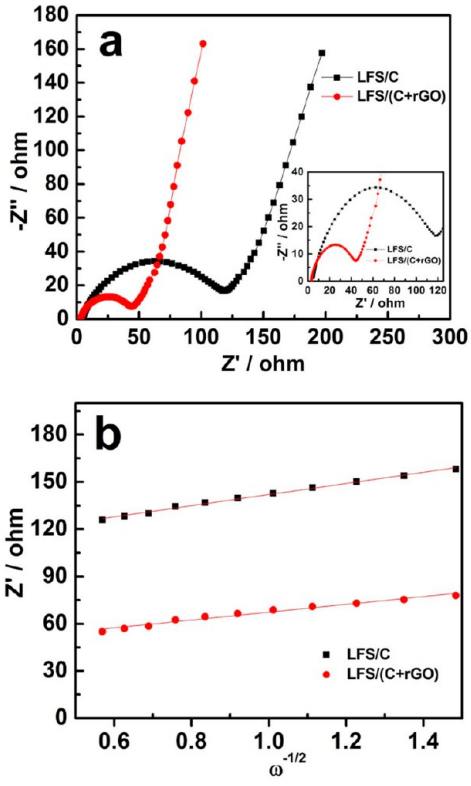

Figure 8. (a) EIS curves and (b) relationship between Z' and $\omega^{-1/2}$ in the low frequency region of LFS/C and LFS/(C+rGO) electrodes.

Both curves in Figure 8 are composed of a small intercept at the high frequency region (inset of Figure 8a), a depressed semicircle at the medium frequency region, and a straight sloping line in the low frequency region. The intercept at the Z' axis represents the ohmic resistance (R_C), corresponding to the resistance of the electrolyte. The semicircle is related to the charge transfer resistance (R_{ct}) and the double-layer capacitance between the electrolyte and cathode (C_{dl}). The inclined line is the Warburg impedance (Z_w), which is associated with Li^+ ion diffusion in the cathode active particles. The higher the charge-transfer resistance R_{ct}, the slower the kinetics of the cell

dx.doi.org/10.1021/am402434n | ACS Appl. Mater. Interfaces 2013, 5, 12304−12309

reactions is. Such EIS curves can be fitted by an equivalent circuit composed of "R(C(RW))" using the ZSimpWin program.[1] According to the fitting results (see Table 1), the

Table 1. EIS Parameters of LFS/C and LFS/(C+rGO) Samples

samples	R_{ct} (Ω)	δ (Ω $S^{1/2}$)	i (mA cm^{-2})	D_{Li} (cm^2 s^{-1})
LFS/C	77.5	35.24	0.332	1.2×10^{-11}
LFS/(C+rGO)	25.4	24.81	1.013	2.4×10^{-11}

charge-transfer resistance can be greatly decreased after rGO incorporation; that is, compared to LFS/C electrode with a R_{ct} value of 77.5 Ω, LFS/(C+rGO) shows a lower R_{ct} value of 25.1 Ω, indicative of a faster kinetics in electrochemical reactions. The exchange current density (i) and the diffusion coefficient of lithium ions (D_{Li}) can be obtained according to the following equations:[3,24,32]

$$i = RT/nFR_{ct} \quad (1)$$

$$D_{Li} = R^2T^2/2A^2n^4F^4C_{Li}{}^2\delta^2 \quad (2)$$

where R is the gas constant, T is the absolute temperature, A is the surface area of the cathode, n is the number of electrons per molecule during oxidation, F is the Faraday constant, C_{Li} is the concentration of lithium ion, and δ is the Warburg coefficient which is related to Z':[3,24,32]

$$Z' = R_C + R_{ct} + \delta\omega^{-1/2} \quad (3)$$

where ω is the angular frequency in the low frequency region, both R_C and R_{ct} are kinetics parameters independent of frequency, so δ is the slope for the plot of Z' versus the reciprocal square root of the lower angular frequencies ($\omega^{-1/2}$). To obtain the Warburg coefficient (δ), the linear fitting of Z' versus $\omega^{-1/2}$ is shown in Figure 8b. All the parameters are listed in Table 1. The results show that, with rGO incorporation, the exchange current density (i) and the diffusion coefficient of lithium ions (D_{Li}) were increased from 0.332 mA cm^{-2} and 1.2×10^{-11} cm^2 s^{-1} to 1.013 mA cm^{-2} and 2.4×10^{-11} cm^2 s^{-1}, respectively. The increased diffusion coefficient of lithium ions (D_{Li}) can be attributed to the reduced crystal size, good particle dispersion, and the improved conductive network between LFS particles connected by rGO and amorphous carbon, and results in a better electrochemical performance for LFS/(C+rGO) electrode.

Raman spectroscopy has been recognized as one of the most sensitive tools for studying the structural properties of carbonaceous materials.[33,34] As shown in Figure 9, two intense broad bands (~1300 and 1590 cm^{-1}) are assigned to the disorder-induced D-line (D-band) and the Raman-active e_{2g} G-line (G-band) of the residual carbon in both samples, respectively. D/G band intensity ratio varies with the structure of the carbon. The lower the D/G band intensity ratio, the higher the electronic conductivity of the residual carbon is.[34] Obviously, after rGO-incorporation, the D/G band intensity ratio decreases, indicative of an increased electronic conductivity, which is in good agreement with the result from electronic conductivity measurements (1.5×10^{-3} S cm^{-1} for LFS/(C+rGO), but 7.1×10^{-4} S cm^{-1} for LFS/C). Additionally, LFS has a series of Raman bands at ~550 and 900 cm^{-1}, assigned to internal bending and stretching vibrations of the SiO_4-tetrahedra, respectively.[35] However, it is hardly to distinguish these Raman bands from the present

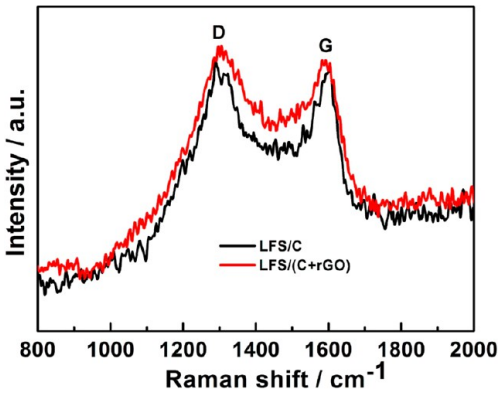

Figure 9. Raman spectra of LFS/C and LFS/(C+rGO) powders.

Raman patterns, because the uniformly coated carbon reduces the optical skin depth of the incident laser so that the penetration depth inside LFS is too short to be effective for data collection. The small SiO_4/C band intensity ratio for both LFS/C and LFS/(C+rGO) indicates a uniform carbon coating on the surface of LFS particles, which agrees well with the results of the TEM images.

4. CONCLUSIONS

Reduced graphene oxide modified Li_2FeSiO_4/C composite was successfully synthesized via a citric acid-based sol–gel method, and its electrochemical performance was investigated. Compared with simple conductive network formed only by amorphous carbon in LFS/C particles, the hybrid conductive network formed by rGO nanosheets and amorphous carbon in LFS/(C+rGO) particles is more favorable for electron migration. EIS results also reveal an increased diffusion coefficient of Li^+ ions in LFS/(C+rGO) electrode. As a result, the rGO modified LFS/C cathode material delivers a higher discharge capacity of 178 mAh g^{-1} with a capacity retention ratio of 94.5% after 40 cycles at 0.1 C, and an average capacity of 119 mAh g^{-1} at 2 C. The present work demonstrates that reduced graphene oxide incorporation is an efficient way for Li_2FeSiO_4 to improve the electrochemical performance.

AUTHOR INFORMATION

Corresponding Author

*Tel: +86-717-6392449. Fax: +86-717-6397559. E-mail: xlyang@ctgu.edu.cn.

Notes

The authors declare no competing financial interest.

ACKNOWLEDGMENTS

This work was supported by the NSFC (Nos. 51302153, 51302152, 51272128, 21175050), Excellent Youth Foundation of Hubei Scientific Committee (2011CDA093), and Key Project of Hubei Provincial Department of Education (No. D20131303). Moreover, the authors are grateful to Dr. Jianlin Li at Three Gorges University for his kind support to our research.

REFERENCES

(1) Zhang, L. L.; Liang, G.; Peng, G.; Zou, F.; Huang, Y. H.; Croft, M. C.; Ignatov, A. *J. Phys. Chem. C* **2012**, *116*, 12401–12408.

(2) Nytén, A.; Abouimrane, A.; Armand, M.; Gustafsson, T.; Thomas, J. O. *Electrochem. Commun.* **2005**, *7*, 156–160.

(3) Peng, G.; Zhang, L. L.; Yang, X. L.; Duan, S.; Liang, G.; Huang, Y. H. *J. Alloys Compd.* **2013**, *570*, 1−6.
(4) Wu, X.; Wang, X.; Zhang, Y. *ACS Appl. Mater. Interfaces* **2013**, *5*, 2510−2516.
(5) Zhou, H.; Einarsrud, M. A.; Vullum-Bruer, F. *J. Power Sources* **2013**, *235*, 234−242.
(6) Gao, K.; Zhang, J.; Li, S. D. *Mater. Chem. Phys.* **2013**, *139*, 550−556.
(7) Armstrong, A. R.; Kuganathan, N.; Saiful Islam, M.; Bruce, P. G. *J. Am. Chem. Soc.* **2011**, *133*, 13031−13035.
(8) Guo, H.; Cao, X.; Li, X.; Li, L.; Li, X.; Wang, Z.; Peng, W.; Li, Q. *Electrochim. Acta* **2010**, *55*, 8036−8042.
(9) Gong, Z. L.; Li, Y. X.; He, G. N.; Li, J.; Yang, Y. *Electrochem. Solid-State Lett.* **2008**, *11*, A60−A63.
(10) Kam, K. C.; Gustafsson, T.; Thomas, J. O. *Solid State Ionics* **2011**, *192*, 356−359.
(11) Hao, H.; Wang, J.; Liu, J.; Huang, T.; Yu, A. *J. Power Sources* **2012**, *210*, 397−401.
(12) Huang, X.; Li, X.; Wang, H.; Pan, Z.; Qu, M.; Yu, Z. *Electrochim. Acta* **2010**, *55*, 7362−7366.
(13) Huang, B.; Zheng, X.; Lu, M. *J. Alloys Compd.* **2012**, *525*, 110−113.
(14) Kucinskis, G.; Bajars, G.; Kleperis, J. *J. Power Sources* **2013**, *240*, 66−79.
(15) Pei, S.; Cheng, H. M. *Carbon* **2012**, *50*, 3210−3228.
(16) Ding, Y.; Jiang, Y.; Xu, F.; Yin, J.; Ren, H.; Zhuo, Q.; Long, Z.; Zhang, P. *Electrochem. Commun.* **2010**, *12*, 10−13.
(17) Bi, H.; Huang, F.; Tang, Y.; Liu, Z.; Lin, T.; Chen, J.; Zhao, W. *Electrochim. Acta* **2013**, *88*, 414−420.
(18) Hu, L. H.; Wu, F. Y.; Lin, C. T.; Khlobystov, A. N.; Li, L. J. *Nat. Commun.* **2013**, *4*, 1687(1−7).
(19) Liu, H.; Yang, G.; Zhang, X.; Gao, P.; Wang, L.; Fang, J.; Pinto, J.; Jiang, X. *J. Mater. Chem.* **2012**, *22*, 11039−11047.
(20) Rui, X.; Sim, D.; Wong, K.; Zhu, J.; Liu, W.; Xu, C.; Tan, H.; Xiao, N.; Hng, H. H.; Lim, T. M.; Yan, Q. *J. Power Sources* **2012**, *214*, 171−177.
(21) Zhang, L.; Wang, S.; Cai, D.; Lian, P.; Zhu, X.; Yang, W.; Wang, H. *Electrochim. Acta* **2013**, *91*, 108−113.
(22) Zhang, W.; Zeng, Y.; Xu, C.; Xiao, N.; Gao, Y.; Li, L. J.; Chen, X.; Hng, H. H.; Yan, Q. *Beilstein J. Nanotechnol.* **2012**, *3*, 513−523.
(23) Hummers, W. S.; Offeman, R. E. *J. Am. Chem. Soc.* **1958**, *80*, 1339.
(24) Yang, J.; Kang, X.; Hu, L.; Gong, X.; He, D.; Peng, T.; Mu, S. *J. Alloys Compd.* **2013**, *572*, 158−162.
(25) Wang, L.; Wang, H.; Liu, Z.; Xiao, C.; Dong, S.; Han, P.; Zhang, Z.; Zhang, X.; Bi, C.; Cui, G. *Solid State Ionics* **2010**, *181*, 1685−1689.
(26) Wu, K.; Yang, J. *Mater. Res. Bull.* **2013**, *48*, 435−439.
(27) Rui, X.; Zhu, J.; Sim, D.; Xu, C.; Zeng, Y.; Hng, H. H.; Lim, T. M.; Yan, Q. *Nanoscale* **2011**, *3*, 4752−4758.
(28) Lv, D.; Wen, W.; Huang, X.; Bai, J.; Mi, J.; Wu, S.; Yang, Y. *J. Mater. Chem.* **2011**, *21*, 9506−9512.
(29) Chen, Z.; Qiu, S.; Cao, Y.; Qian, J.; Ai, X.; Xie, K.; Hong, X.; Yang, H. *J. Mater. Chem. A* **2013**, *1*, 4988−4992.
(30) Wu, X.; Jiang, X.; Huo, Q.; Zhang, Y. *Electrochim. Acta* **2012**, *80*, 50−55.
(31) Nytén, A.; Kamali, S.; Häggström, L.; Gustafsson, T.; Thomas, J. O. *J. Mater. Chem.* **2006**, *16*, 2266−2272.
(32) Yan, Z.; Cai, S.; Zhou, X.; Zhao, Y.; Miao, L. *J. Electrochem. Soc.* **2012**, *159*, A894−A898.
(33) Lespade, P.; Marchand, A.; Couzi, M.; Cruege, F. *Carbon* **1984**, *22*, 375−385.
(34) Baddour-Hadjean, R.; Pereira-Ramos, J.-P. *Chem. Rev.* **2010**, *110*, 1278−1319.
(35) Kolesov, B. A.; Geiger, C. A. *Phys. Chem. Miner.* **1998**, *25*, 142−154.